Proceedings of the XVII ECSMGE-2019
Geotechnical Engineering foundation of the future
ISBN 978-9935-9436-1-3

doi: 10.32075/17ECSMGE-2019-1024

XVII European Conference
ECSMGE 2019
Reykjavik
on Soil Mechanics
and Geotechnical Engineering

Experimental study on liquefaction characteristics of saturated coral sand in Nansha Islands under cyclic loading

Etude expérimentale sur les caractéristiques de liquéfaction des sables coralliens Nansha saturés sous charge cyclique

W. J. MA
Institute of Geotechnical Engineering, Nanjing Tech University, Nanjing, China

G. X. CHEN, Q. WU
Institute of Geotechnical Engineering, Nanjing Tech University, Nanjing, China

ABSTRACT: Undrained cyclic traxial tests are carried out on saturated coral sand in Nansha Islands, South China Sea. The experiment aims at investigating the characteristics of pore water pressure, axial strain, effective stress path and cyclic strength about coral sand under different D_r and σ'_{3c} .The differences between coral sand and Fujian sand about liquefaction characteristic are also discussed. The test results indicate that the development of pore water pressure (Δu) of coral sand is different from siliceous sand. A modified Seed model is proposed to describe the the development of pore water pressure of coral sand. The accumulative energy dissipation of coral sand required to trigger the liquefaction is greater than Fujian sand at the same *CSR*. Axial strain (ε_{DA}) of coral sand has no sudden enlargement during cyclic loading and the amplitude of ε_{DA} increases with the loading time. Compared with Fujian sand, coral sand has a greater fluctuation in especially when approaching σ'_{3c} . 'Transient liquefaction' can be observed in the test. The liquefaction resistance of coral sand increases with increasing of D_r and σ'_{3c} .The liquefaction resistance of coral sand is basically higher than siliceous sand.

RÉSUMÉ: Une série d'essais de chargement cyclique non drainants pour les sables coralliens de récifs Nansha saturés ont été effectuées à l'aide d'appareils triaxiaux dynamiques GDS, et les effets de la densité relative D_r et la pression initiale de confinement σ'_{3c} sur la pression d'eau ultra-interstitielle, le développement des déformations, la trajectoire de contrainte effective et les caractéristiques de résistance dynamique des sables coralliens saturés ont été étudiés, et aussi les caractéristiques de liquéfaction du sable de corail et du sable de Fujian. L'expérience montre que le mode de développement du Δu de la pression d'eau ultra-interstitielle du sable de corail est différent de celui du sable de quartz, et peut être caractérisé par le modèle Seed modifié. La dissipation d'énergie accumulée de la liquéfaction de sable de corail est beaucoup plus grande que celle du sable de Fujian. La souche axiale ε_{DA} du sable de corail augmente graduellement avec l'augmentation de la vibration cyclique, et le phénomène de l'augmentation rapide ne se produira pas. Par rapport à la fluctuation caractéristique de Δu de sable de Fujian, la fluctuation des Δu de sable de corail est plus grande, et quand le Δu est proche de σ'_{3c} , la fluctuation augmente évidemment, qui produit le phénomène de «liquéfaction instantanée». La force dynamique du sable de corail augmente avec l'augmentation du D_r et du σ'_{3c} . La force dynamique du sable de corail est plus grande que celle du sable de quartz.

Keywords: cyclic triaxial test; generation pattern of excess pore pressure; cycle resistance ratio

1 INTRODUCTION

Coral sand is a special marine soil formed by the physical, biological and chemical interactions of the skeleton of marine organisms. The content of calcium carbonate in coral sand reachs approximately 90%, which is much higher than that in calcareous sand(Yu, 1999). Therefore, coral sand is a veritable calcareous sand. Coral sand has the characteristics of high friction angle, low strength, fragile, irregular shape and internal porosity due to its special formation process(Zhu, 2014; Chen, 2005). It is expected that coral sand has distinct dynamic properties compared with terrigenous quartz sand(Olson, 2012). There are plenty of coral reefs with high seismic risk near the South China Sea. However, limited work has been conducted on the seismic safety of coral reefs in the South China Sea. The primary problem of preventing and mitigating earthquake disasters in the South China Sea islands and reefs engineering is to determine the possibility of liquefaction of the islands and reefs engineering sites. Therefore, the dynamic characteristics of coral reefs in the South China Sea Islands is a basic scientific problem that needs to be solved urgently. According to the recent earthquake damage data(Guam earthquake in 1993, Hawaii earthquake in 2006, Haiti earthquake in 2010), the saturated coral sand has serious liquefaction phenomena. A series of laboratory experiments have been conducted by many scholars to study the liquefaction behavior of coral sand. Hyodo *et al*.(1998) carried out a series of undrained dynamic triaxial tests on Dogs Bay coral sand and Toyoura sand, compared the dynamic strength between the two sands, and established the relationship between phase transformation strength and dynamic strength of Dogs Bay coral sand. Salem *et al*.(2013) point out that the pore pressure criterion was more reasonable than the strain criterion in judging the liquefaction of Dabaa coral sand. Sharma *et al*.(2006) carried out a series of dynamic triaxial tests on Goodwyn and Ledge Point coral sands to investigate the volume changes of soil under one-way and two-way loading, and compared the cyclic shear strength and strain magnitude at failure. Yu & Wang(1999) studied the deformation characteristics of coral sand in Xisha Islands subjected to the loading of wave. They concluded that the plastic deformation of coral sand was easy to occur during cyclic loading, which was related to the high compressibility of coral sand. The above studies have made different analysis on the liquefaction characteristics of coral sands, but the research on the dynamic characteristics of the saturated coral sand in Nansha Islands is still insufficient. It is necessary to make further experimental on the coral sand in Nansha Islands. The differences in the dynamic characteristics of coral sand and quartz sand need to be further discussed.

A series of undrained cyclic triaxial tests were carried out on saturated coral sands of Nansha Island with different relative densities D_r and initial confining pressures σ'_{3c} by using GDS dynamic triaxial apparatus. The pore pressure development model, deformation characteristics and liquefaction resistance characteristics were analyzed. A few of cyclic loading tests of saturated Fujian sands were carried out for comparision.

2 APPARATUS AND MATERIAL

2.1 Dynamic traxial apparatus

The experiment was carried out by the GDS dynamic traxial apparatus which is shown in Figure 1. The instrument consists of a computer system, a digital control system, a dynamic control system for axial force and displacement, and two standard pressure/volume controllers. The maximum axial load is ± 5 kN and the accuracy is 0.001 kN. The maximum pressure can reach to 2 MPa. The range of maximum axial displacement is 100 mm and the displacement precision is 0.07% F.S (full scale).

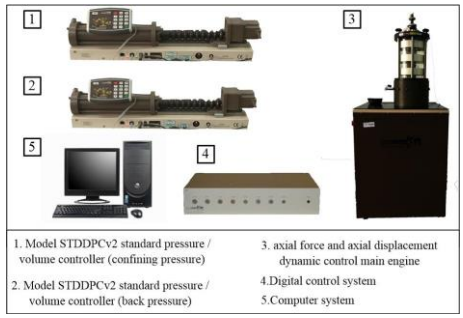

Figure 1. GDS dynamic traxial test apparatus

2.2 Testing material

The tested coral sand was taken from a reef in Nansha islands. Figure 2 shows the scanning image of coral sand by electron microscope.

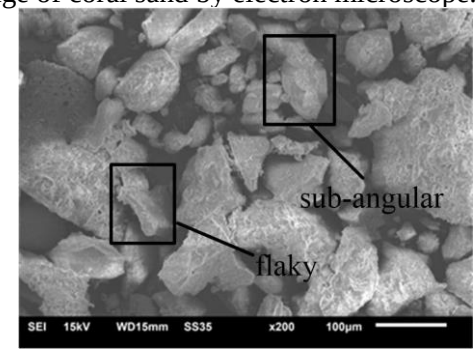

Figure 2. SEM (Scanning electronic microscope) graphs of coral sand in Nansha Islands

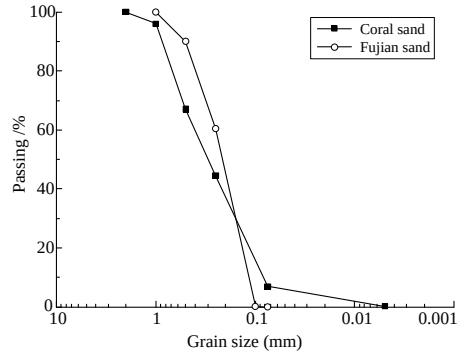

Figure 3. Grain size distribution curves of coral sand

From the picture, it can be seen that the shape of coral sand particles are almost sub-angular and flaky. The surface of the particles is rough. The mean particle size of coral sand is 0.31mm, specific coefficinet is 2.8, the maximum and minimum void ratio are 1.72 and 0.99, respectively. The Fujian sand used in the test is a typical quartz sand in China with round grains and smooth surface. The grading curve is shown in Figure 3.

Table 1. Summary of tests schemes

No.	D_r/%	$D_{r(con)}$/%	σ'_{3c} /kPa	*CSR*
S1	45	48.02	50	0.15
S2	45	48.35	50	0.2
S3	45	47.84	50	0.25
S4	45	50.50	100	0.15
S5	45	51.04	100	0.2
S6	45	50.11	100	0.25
S7	45	52.92	200	0.15
S8	45	52.05	200	0.2
S9	45	54.40	200	0.25
S10	30	35.92	100	0.15
S11	30	36.85	100	0.2
S12	30	36.61	100	0.25
S13	60	65.04	100	0.15
S14	60	64.03	100	0.2
S15	60	64.42	100	0.25
F16	45	51.20	100	0.1
F17	45	51.67	100	0.12
F18	45	52.12	100	0.15

NOTE：S: Coral sand，F: Fujian sand.

3 TEST PROCEDURES

All specimens were prepared using the dry deposition method. In this method, the specimens were prepared by placing soils in five equal-mass layers in the mold, and a dry uniform sand was poured into the molds. After the specimen was placed in the cell, the cell pressures of 20 kPa were applied. The two stages of saturation (carbon dioxide flushing and de-aired water flushing) were then carried out. Each specimen was back-pressurized to 400 kPa for complete saturation, with a Skempton's B-

value of 0.97 or higher. After complete saturation, all the specimens were isotropically consolidated with different confining pressures according to the experimental scheme. Detailed experimental scheme is shown in Table 1.

4 ANALYSIS

Taking the test result of soil sample No. S2 as an example, the measured time history curves of pore pressure, axial strain and deviatoric stress of coral sand are given in Figure 4. The excess pore water pressure Δu of coral sand increases continuously with cycle number N, and the double amplitude strain ε_{DA} develops gradually. σ_d can keep constant during the generation of excess pore water pressure, and diverges after the sample liquefies, i.e., when the effective stress of the sample is approaching to zero. This indicates that the instrument has good performance and the test results are credible.

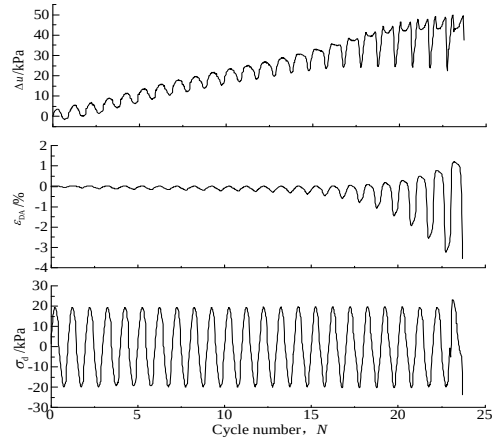

Figure 4. Measured time histories of typical specimen test results

4.1. Comparative analysis of test results of two kinds of sand

The time history curves of Δu when CSR = 0.15 for coral sand and Fujian sand are shown in Fig. 5 (a) and 5 (b), respectively. Δu of coral sand reaches σ'_{3c} after 208 cycles, while Δu of Fujian sand reaches σ'_{3c} after 4 cycles, which means that coral sand has stronger liquefaction resistance than Fujian sand.

Fig. 5 (c) and 5 (d) show the developments of excess pore water pressure in two sands when the cycle number caused liquefaction N_L of coral sand and Fujian sand are alomst identical. The results indicate that the accumulated excess pore water pressure generally increases with the increase in number of loading cycle in each sample. However, excess pore water pressure generated in the coral sand has more fluctuations that that generated in the Fujian sand when the effective stress is approaching zero. This is because the coral sand has stronger dilatancy than the Fujian sand. The coral sand presents the phenomenon of "instantaneous liquefaction" (Groot, 2006). That is, after initial liquefaction, the Δu of the soil is equal to only at some instants, but the soil structure is not completely destroyed.

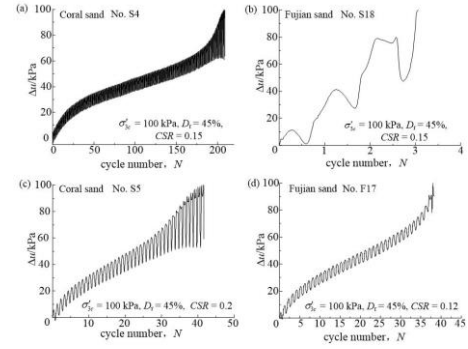

Figure 5. Comparison of the time histories of the pore water pressure of coral sand and Fujian sand

Fig. 6 is the axial strain ε_{DA} curve of two sands. It should be noted that ε_{DA} of coral sand produces obvious elastic axial deformation at the begining. The ε_{DA} increases gradually with N until liquefaction, and no sudden enlargement occur like Fujian sand. Because of the irregular shape and rough surface of coral sand particles, there are many contact points between the particles, which makes the soil structure more stable. With the increase of Δu, the contact force between particles decreases gradually. Due to the high void ratio and the influence of a small amount of particle breakage, the reorganization

phenomenon of particle is more likely to occur between particles, and the soil structure becomes relatively stable. Thus, the increase of pore pressure is inhibited, which means coral sand need more cycle number to liquefaction.

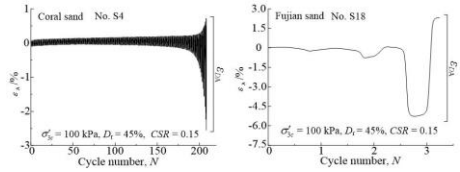

Figure 6. Comparison of the time histories of axial strains for coral sand and Fujian sand

The stress-strain relationship of two sands are shown in Fig. 7. The area of hysteresis loop of Fujian sand is very small before liquefaction, but suddenly becomes larger when liquefied. However, the area of hysteresis loop of coral sand is gradually increased during cyclic loading, and the area of hysteresis loop is much larger than that of Fujian sand. This indicates that the energy dissipation modes of two sands is different.

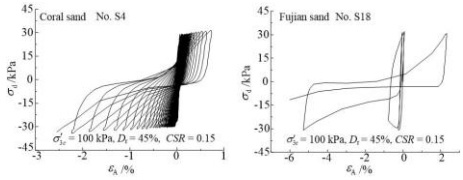

Figure 7. Comparison of the curves of stress-strain for coral sand and Fujian sand

Figueroa(1994) proposed to describe the energy dissipation of soil element by the area of hysteresis loop. The energy dissipation of two sands calculated by the same consolidation conditions and *CSR* is shown in Figure 8.

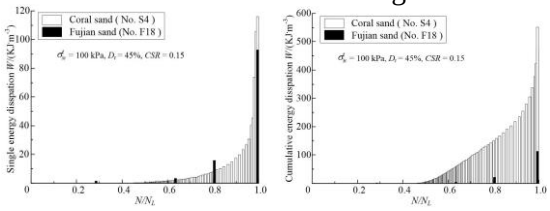

Figure 8. Comparison of the energy dissipations for coral sand and Fujian sand

The single energy dissipation of coral sand increases gradually with cycle number, while that of Fujian sand is almost zero in the early cycles, and increases rapidly during liquefaction. It is noteworthy that the cumulative energy dissipation of coral sand during liquefaction is as high as 551 kJ/m^3, while that of Fujian sand is only 113 kJ/m^3. This can be explained that coral sand has strong structure and needs more energy to make the soil structure destroyed.

4.2. Characteristics of pore pressure

The pore pressure ratio R_u is defined as the ratio of peak value of Δu for each cycle to σ'_{3c}. Fig. 9 shows the relationship between R_u and N/N_L for different *CSR*. It is Obvious that *CSR* has a significant effect on the development of R_u. Lee and Albaisa(1974) give the upper and lower boundaries of R_u for the Monterey sand, see the dotted line in Figure 10. Obviously, the upper and lower boundaries of R_u for quartz sand do not apply to coral sand.

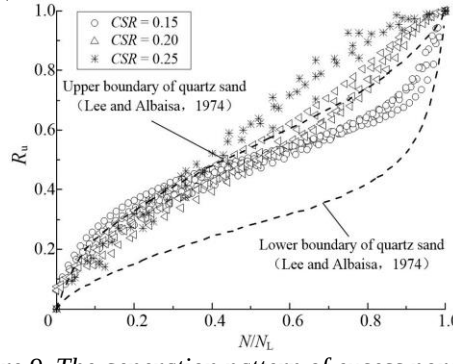

Figure 9. The generation pattern of excess pore pressure for coral sand (CSR = 0.15、0.2、0.25)

In order to clearly observe the development pattern of R_u, figure 11 shows the relationship between R_u and N/N_L at a given *CSR*. For different D_r and σ'_{3c}, the development of R_u are identical as the same *CSR* applied to the specimen. Seed(1976) proposed a solution for predicting R_u as a function of N/N_L which can be expressed as:

$$R_u = \frac{1}{2} + \frac{1}{\pi}\arcsin\left(2\cdot\left(N/N_L\right)^{1/\theta} - 1\right) \qquad (1)$$

where θ is a parameter dependent on the soil type. Subsequently, Booker *et al.*(1976) simplified the formula as follows:

$$R_u = \frac{2}{\pi}\arcsin\left(N/N_L\right)^{1/2\theta} \quad (2)$$

The fitting result of coral sand is shown in the dotted line of Figure 10 by Eqs (2). The results indicate the Seed predictions correspond well with the measurements at low CSR, i.e., CSR =0.15,0.2 ; However, at hight CSR, i.e., CSR=0.25, there is a significant difference between the predictions and measurements. Thus, it is necessary to propose a modified Seed model to describe the pore pressure development of coral sand:

$$R_u = a\times\frac{2}{\pi}\arcsin\left(N/N_L\right)^{1/2\theta} + b\times\arctan\left(N/N_L\right) \quad (3)$$

where *a*, *b* and θ are three fitting parameters. The fitting parameters listed in Table 2 are obtained. The fitting curves are shown in Figure 10.

The modified Seed model has a good result in describing the development R_u of coral sand, the results show that *R*-squared is greater than 0.98. The variation of model parameters has obvious rules: *a* and θ decreases with the increase of *CSR*, while *b* increases with the increase of *CSR*. Therefore, *CSR* has great influence on the pore pressure development pattern of coral sand.

Table 2. Fitting coefficients of the modified Seed model

CSR	***a***	***b***	θ	R^2
0.15	1.381	-0.489	1.047	0.985
0.20	0.964	0.151	0.869	0.980
0.25	-0.168	1.492	0.403	0.995

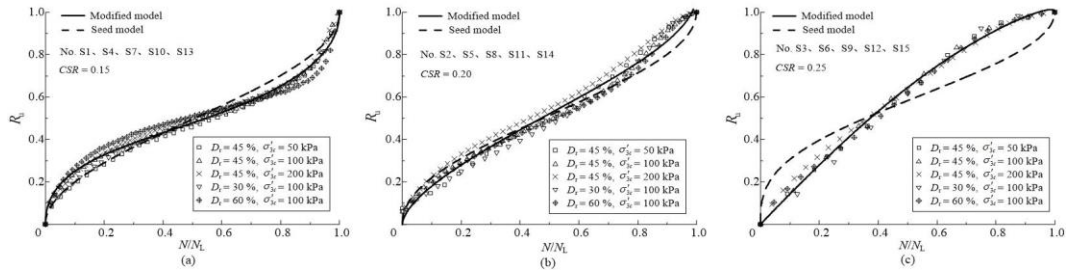

Figure 9. Test data and the prediction values of the corrected Seed model for generation of excess pore pressure of coral sand at the various CSR

4.3. Characteristics of axial strain

Fig. 10 shows the curves of double axial strain ε_{DA} of coral sand at *CSR* = 0.15, 0.2 and 0.25. The development trend of ε_{DA} becomes faster with the increase of *CSR*. It can be found that when *CSR* = 0.15, ε_{DA} need 100 cycles to reach 5%, which means that the coral sand will not liquefy under the minor earthquake; when *CSR* = 0.25 and the soil sample is in the state of low confining pressure and medium density, ε_{DA} can reach to 5% in 12 cycles, which means that liquefaction of coral sand will occur easily under strong earthquake.

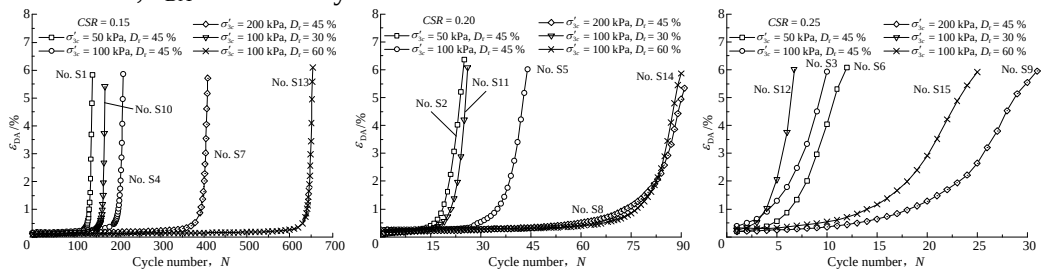

Figure 10. Double strain development of coral sand at the various CSR

4.4. Characteristics of liquefaction resistance

The liquefaction resistance of soil is an important index. Taking pore pressure ratio R_u = 100% as the liquefaction standard for coral sand, the relationship between *CSR* and N_L is given in Fig. 11.

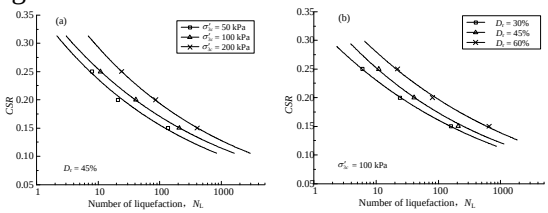

Figure 11. Cyclic strength curves of coral sand (a) The influnce of σ'_{3c} on Cyclic strength; (b) The influnce of D_r on Cyclic strength

It can be observed that the liquefaction resistance curves of saturated coral sand increases with the increase of σ'_{3c}. The reason is that σ'_{3c} has significant effect on the contact force between particles. Moreover, the particle arrangement will become closer at higher σ'_{3c} that leads to the increase of D_r because of the high compressibility. D_r also has a great influence on the liquefaction resistance curves of coral sand, which is consistent with the property of quartz sand.

There is a strong relationship between the cycle number of liquefaction gaining from laboratory test and the earthquake magnitude. Table 3 shows the relationship between σ'_{3c}, $D_{r(con)}$ and *CRR* at N_L of 15 and 20, which are proposed by Seed(1985) and Martin(1975) for a magnitude 7.5 earthquake, respectively.

Table 3. The relationship between σ'_{3c} and $D_{r(con)}$ versus CRR

$D_{r(con)}$/%	σ'_{3c}/kPa	*CRR*	
		15 cycle	20cycle
48.07	50	0.22	0.208
50.55	100	0.242	0.229
53.12	200	0.273	0.258
36.46	100	0.216	0.207
64.5	100	0.263	0.252

Salem has proposed the use of parameter $\sigma'_{3c} \times D_r^{-0.55}$ to describe the impact of D_r and σ'_{3c} on *CRR*. Accordingly, the parameters are modified by introducing the parameter $(\sigma'_{3c}/100)^{\alpha} \times D_{r(con)}^{0.5-\alpha}$, to describe the influence of σ'_{3c} and $D_{r(con)}$ of *CRR*. For the coral sand used in this experiment, when the value of α is 0.14, this parameter has a strong linear correlation with *CRR*, The result is shown in Figure 12.

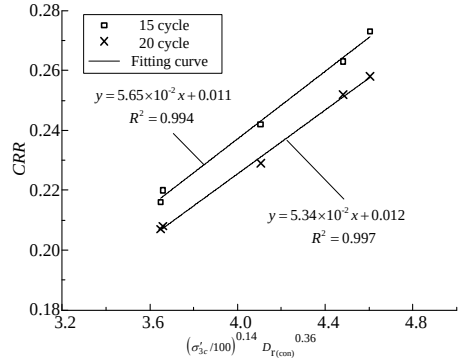

Figure 12. The relationship of σ'_{3c} 、 $D_{r(con)}$ and CRR

The liquefaction resistance curves of different coral sand and quartz sand under similar conditions are compared in Figure 13. Overall, coral sand has stronger liquefaction resistance than quartz sand. As mentioned before, it is due to the rapid dissipation of pore water, the slow increase of axial strain and large energy dissipation of coral sand during liquefaction.

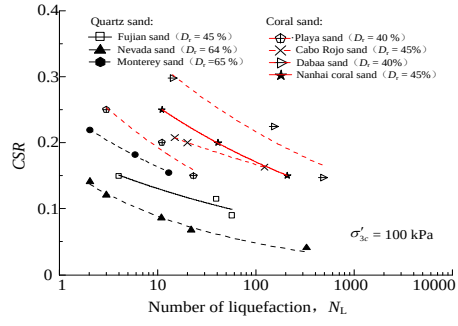

Figure 13. Comparison of the cyclic strengths between different types of coral sand and siliceous sand

5 CONCLUSIONS

1. For coral sand, when Δu of coral sand reaches σ'_{3c}, Δu will fluctuate greatly, and the phenomenon of "instantaneous liquefaction" will appear. The sudden increase of ε_{DA} will not occur, and the energy dissipation in the process of liquefaction is larger, which indicates that coral sand is more difficult to liquefy.
2. According to the pore pressure development characteristics of coral sand, a modified Seed model is proposed to describe the pore pressure development of coral sand.
3. Compared with quartz sand, coral sand has higher liquefaction resistance. The liquefaction resistance cuvres of coral sand increases with the increase of D_r and σ'_{3c}. The parameters $(\sigma'_{3c}/100)^{\alpha} \times D_{r(con)}^{0.5-\alpha}$ can be used to describe the effect of $D_{r(con)}$ and σ'_{3c} on *CRR*.

6 ACKNOWLEDGEMENTS

The study in this paper is supported by the the Project of the National Natural Science Foundation of China (51678299). This financial support is gratefully acknowledged.

7 REFERENCES

Zhu C, Chen H, Meng Q. 2014. Microscopic characterization of intra-pore structures of calcareous sands. *Rock and Soil Mechanics* **35**(7), 1831-1836.

Chen H, Wang R, LI J. 2005. Grain shape analysis of calcareous soil. *Rock and Soil Mechanics* **26**(9), 1389-1392.

Olson S M, Green R A, Lasley S. 2012. Documenting Liquefaction and Lateral Spreading Triggered by the 12 January 2010 Haiti Earthquake. *Earthquake Spectra* **27**(S1), S93-S116.

Hyodo M, Hyde A F L, Aramaki N. 1998. Liquefaction of crushable soils. *Géotechnique* **48**(4), 527-543.

Salem M, Elmamlouk H, Agaiby S. 2013. Static and cyclic behavior of North Coast calcareous sand in Egypt. *Soil Dynamics and Earthquake Engineering* **55**, 83-91.

Sharma S S, Ismail M A. 2006. Monotonic and cyclic behavior of two calcareous soils of different origins. *Journal of Geotechnical and Geoenvironmental Engineering* **132**(12), 1581-1591.

Yu H, Wang R. 1999. Experimental study on dynamic strength of calcareous sand. *Rock and Soil Mechanics* **20**(4), 6-11.

Groot M B D, Bolton M D, Foray P, et al. 2006. Physics of liquefaction phenomena around marine structures. *Journal of Waterway Port Coastal & Ocean Engineering* **132**(4), 227-243.

Figueroa J L, Saada A S, Liang L. 1994. Evaluation of Soil Liquefaction by Energy Principles. *Journal of Geotechnical Engineering* **120**(9), 1554-1569.

Lee K L, Albaisa A. 1974. Earthquake induced settlements in saturated sands. *Journal of Engineering & Applied Sciences* **2**(4).

Seed H B, Lysmer J, Martin P P. 1976. Pore-Water Pressure Changes during Soil Liquefaction. *Journal of the Geotechnical Engineering* **102**(4):323-346.

Booker, J R, Rahman, M S, Seed. H B. 1976. GADFLEA—A computer program for the analysis of pore pressure generation and dissipation during cyclic or earthquake loading[R]. Earthquake Engineering Research Center, Univ. of California at Berkeley, Berkeley, Calif.

Seed H B, Tokimatsu K, Harder L F. 1985. Influence of SPT Procedures in Soil Liquefaction Resistance Evaluations. *Journal of Geotechnical Engineering* **111**(12), 1425-1445.

Martin G R, Finn W D L, Seed H B. 1975 Fundamentals of liquefaction under cyclic loading. *Journal of the Geotechnical Engineering* **101**(5), 423-438.

Brandes H G. 2011. Simple shear behavior of calcareous and quartz sands. *Geotechnical & Geological Engineering* **29**(1), 113-126.

Sandoval E A, Pando M A. 2012. Experimental assessment of the liquefaction resistance of calcareous biogenous sands. *Earth Sciences Research Journal* **16**(16), 55-63.

Lavielle T H. 2008. Liquefaction susceptibility of uncemented calcareous sands from Puerto Rico by cyclic triaxial testing. Virginia Tech.